Correlation preparation parameters/activity for microTiO$_2$ decorated with SilverNPs for NOx photodegradation under LED light

Giuseppina Cerrato[a], Federico Galli[c], Daria C. Boffito[b], Lorenza Operti[a], Claudia L. Bianchi[c,*]

[a] Università degli Studi di Torino, Dipartimento di Chimica & NIS Interdept. Centre, via P. Giuria 7, 10125, Torino, Italy
[b] Polytechnique Montréal, Department of Chemical Engineering, C.P. 6079, Centre ville H3C 3A7, Montréal, QC, Canada
[c] Università degli Studi di Milano, Dipartimento di Chimica, via Golgi 19, 20133, Milano, Italy

ARTICLE INFO

ABSTRACT

TiO$_2$ photocatalysts degrade pollutants in both the gas and liquid phase under UV radiation. To widen their application under solar and/or LED light, TiO$_2$ surface decoration with noble metals offers a mean to achieve such a goal. Ag species as a decorating agent improve TiO$_2$-based systems photoactivity and exhibit antibacterial properties under LED light and even in the dark. Ample literature is available on the synthesis of silver nanoparticles (Ag NPs) but few data are available on the interaction of such particles with micrometric samples. Indeed, micrometric samples pose less environmental and health concerns than the nano-sized powders widely adopted. The synthetic routes employed for Ag NPs decoration onto TiO$_2$ clearly influence the photocatalytic activity, in particular referring to both NPs shape and fine structure. Thus, we report the preparation of Ag NPs by an electrochemical method followed by the subsequent decoration onto a micrometric TiO$_2$ (Kronos 1077): different parameters, such as pH and the nature of physical nanoparticle dispersants were taken into account to evaluate their effect on the resulting Ag NPs features. We evaluated the photocatalytic activity towards the photodegradation of NOx under LED light, concluding that the best output was obtained by photocatalysts synthesised at basic pH.

1. Introduction

Capturing renewable sunlight by permanently abducting photons into complex systems capable of storing them and, at the same time, realizing them or transforming them into reactive species would arguably be the Holy Grail of energy utilization of the current century.

Researchers are looking for more efficient ways to store and re-use solar energy. Photocatalysis, still far from being efficient, offers scientists the chance of embracing this challenge [1]. In particular, TiO$_2$ is now seen as an unforsaken vector to attain the objective of an affordable and efficient photocatalyst.

TiO$_2$ undoubtedly possesses alluring characteristics such as long-term mechanical and thermal stability, even under irradiation [2], availability, feasible synthesis and low cost [3]. However, its low efficiency ejects widespread commercial applications. The reason for its inadequacy lies in its wide band-gap (Eg), which limits the irradiation that can be absorbed. Indeed, an Eg $\approx$ 3.2 eV requires $\lambda_{irr} <$ 385 nm, which disqualifies 95% of the solar spectrum. In addition, the high recombination rate of the photogenerated species results in a low production rate of secondary photo-generated reactive compounds [4,5].

Diverse approaches such as coupling TiO$_2$ with other semiconductors [6,7], dye sensitizing [8,9], ion implantation [10], noble metal [4] decoration, doping with heteroatoms [11] now account for several literature data. Among the noble metals, Ag NPs have been a target since they also possess antibacterial properties [12]. However, besides this, AgNPs exhibit the surface plasmon band typical of noble metal NPs, which originates from the Mie absorption in the visible spectrum. When incorporated onto TiO$_2$, its band-gap decreases, opening up the light absorption over a wider light spectrum region. The fundamental mechanism of visible light absorption by TiO$_2$ decorated with Ag identifies with the injection of metal plasmonic electrons into the wide band-gap semiconductor. However, the plasmonic absorption, which is an optical property at the surface/bulk interface, only manifest for NPs bigger than 2 nm. Below this size, quantum effects prevails [13]. The most recent approaches focus on interposing a layer of conductive material between TiO$_2$ and Ag to provide a conductive path for the electrons from the noble metal to the TiO$_2$ surface. For instance, Lang et al. intercalated graphene oxide (GO) nanosheets as bridges between Ag nanocubes and TiO$_2$ nanosheets to provide a conductive path for the electrons from the plasmonic Ag band to the semiconductor [14]. Asapu

---

* Corresponding author.
  E-mail address: claudia.bianchi@unimi.it (C.L. Bianchi).

et al. fabricated core-shell super stable Ag-TiO$_2$-PAH where poly-allylamine hydrochloride (PAH) constitute a polycation layer [15], whereas Jbeli et al. Intercalated a chitosan film that formed an AgCl layer between TiO$_2$ and Ag species [16].

Controlling the dispersion and size of the noble metal over TiO$_2$ is fundamental to both maximize photocatalytic activity by tackling the mass transfer of active primary and secondary photogenerated species, as well limiting the input of catalyst precursors' and solvents in an approach towards sustainability. For instance, Stucchi et al. doped micrometric (110 nm) TiO$_2$ with Ag nanoparticles (NPs) in the weight range from 1 to 20% by means of ultrasound [17]. Zeng et al. synthesized Ag nanowires with TiO$_2$ NPs around them that were stable for several days and degraded acetaldehyde in few minutes in the gas phase under fluorescent light [18].

AgNPs agglomerated electrochemically to control their size is an innovative and interesting approach because it is possible to precisely control the size of Ag. Starowicz et al. polarized a sacrificial anode of Ag and obtained AgNPs of about 20 nm [19]. With the same technique, Rodriguez-Sanchez et al. obtained nanoparticles in the range 2–7 nm in acetonitrile and tetrabutylammonium bromide as electrolyte and stabilizer [19]. TiO$_2$ particle size is another fundamental issue to tackle the benefits of nanotechnology dominate our thinking nowadays. The concerns regarding nano-particles (< 100 nm) deal with inhalation and skin contact of particles that are so small to be potentially not "recognizable" by the human body barriers, thus reaching the organism cells. The number of papers on the subject "TiO$_2$ nanoparticles and toxicity", which raised from 57 (within 2008) to 985 in the last 10 years [Scopus.com source], is a proof of the increasing concern about the effects of nanoparticles on living beings. Concurrently, major national and international agencies in Europe are promoting research on potential adverse effects of nanoparticles [20]. The effects of nano-sized TiO$_2$ on human health have not been fully demonstrated yet, but the first data on the adverse effect of nano-sized TiO$_2$ on animals just became available [21,22].

The authors recently confronted this issue by several papers published on increasing the photoactivity of micro-TiO$_2$ [23–25], whereby doping micro-sized TiO$_2$ the activity increased in the visible range.

Among all the pollutants, nitrogen oxides (NOx) are continuously monitored all over the world and guidelines on the alarm levels of these molecules in air were published by WHO [26] and often recalled in the legislation of single countries worldwide. Photocatalysis with titanium dioxide as a semiconductor seems to be a promising technique to reduce the pollutant concentration due to its powerful oxidation properties. For this reason, the NOx degradation reaction was selected to probe the photocatalytic activity of our samples. Folli et al [27] report a correlation between the maximum NO removal (minimum concentration) with the maximum UV irradiance. Another recent review contribution by Schreck et al. [28] reports about NOx emissions, in particular from the transport sector, as they significantly impact the urban air quality. The band-gap of anatase phase TiO$_2$ is 3.2 eV and the oxidation and reduction potentials of the valance and conduction bands are $+2.95$ V and -0.25 V, respectively. The reduction potential of NO to N$_2$ is $+3.36$ V and the oxidation potential of NO to NO$_3^-$ is -0.934 V indicating that both photooxidation and photoreduction of NO are feasible reactions over TiO$_2$ [29].

In this paper, we report the electrochemical synthesis of Ag NPs together with their subsequent deposit by incipient wetness on micrometric TiO$_2$. During the synthesis of the catalyst, the pH was varied in the 4–12 range, observing exceptional catalytic performance (90% NOx conversion in 1 h) under LED light for the sample obtained at pH = 14 and PVP/Ag + molar ratio = 3.

2. Experimental

2.1. Silver nanoparticles preparation

Ag NPs were prepared from an AgNO$_3$, polyvinyl pyrrolidone (PVP) and KNO$_3$ solution. KNO$_3$ ($\geq$ 99.0%) and PVP (average molecular weight = 40 000) were purchased from Sigma Aldrich and were employed with no further purification. 100 mL of a 30 g/L AgNO$_3$ solution were placed into a beacker containing 1 g of KNO$_3$ and a weighted amount of PVP. KNO$_3$ solution was added as supporting electrolyte. PVP acted as physical nanoparticle dispersant [30] and we varied its concentration to gauge the effect of PVP on the synthesis. We varied the dispersant to understand its influence on the stabilization of Ag NPs. We selected polyvinyl alcohol (PVA) (average molecular weight = 9000–10000, 80% hydrolysed, Sigma Aldrich) [31] and polyacrylic acid (PAA, sodium salt, average molecular weight = 8000, Sigma Aldrich) [32]. The counter and working electrode were two platinum foils (40 mm x 20 mm), while the reference electrode was a saturated calomel electrode (SCE). To protect SCE from AgCl precipitation, we used double bridge filled up with a saturated KNO$_3$ solution, which acted as the second electrolyte.
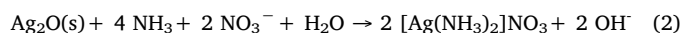
AUTOLAB potentiostat coupled with Nova software determined the reduction potential for each test through cyclovoltammetry (CV). The cyclic staircase started from 0.4 V, reached a lower potential -0.2 V, increased until 1.0 V, and returned to 0.4 V. The reductive current obtained from CVs was almost constant from $+0.3$ V to -0.2 V, therefore it was decided to synthesize Ag nanoparticles at $+0.2$ V, to maximize silver production and to avoid, at the same time, to deposit metallic silver on the electrode. We observed that in this condition, after 10 min, silver only deposited on the working electrode. Therefore, we set the duration of each synthesis to 10 min.

We also modified the pH of the solution after the electrochemical synthesis with either HNO$_3$ or NH$_4$OH, to study the influence of pH on the Ag nanoparticles structure/morphology and verify its possible influence of the final photocatalytic performance.

2.2. Catalyst synthesis

During the electrochemical synthesis, the colour of the mixture gradually shifted from white to yellow and became cloudier, thus indicating the formation of nanoparticles. [3].

We then added NH$_4$OH to the silver nanoparticles (Ag NPs) solution to a pH of 12 to form NH$_3$. Ammonia stabilizes the dopant in the solution avoiding the formation of Ag$_2$O precipitate according to Tollens reaction (1) and (2):

$$AgNO_3 + 2\ OH^- \rightarrow Ag_2O(s) + 2\ NO_3^- + H_2O \quad (1)$$

$$Ag_2O(s) + 4\ NH_3 + 2\ NO_3^- + H_2O \rightarrow 2\ [Ag(NH_3)_2]NO_3 + 2\ OH^- \quad (2)$$

We then suspended TiO$_2$ (Kronos 1077) in 6 mL of acetone (HPLC grade, Sigma Aldrich). We added the Ag NPs aqueous solution to the suspension to obtain an AgNPs mass loading of 8% (value optimized in previous works). The solution was kept under stirring for 24 h, at a temperature of 40 °C. After, we raised the temperature to 80 °C for 2 h. At the end of the impregnation, we removed water by evaporation and heated the mixture to 100 °C A furnace calcined the powder at 400 °C for 2 h under static atmosphere.

Here we compare 7 catalysts (Table 1) prepared with different conditions. Sample 7 was prepared in the same condition of sample 6 but with 5 times the reagents amount and the volumes (500 mL of AgNO$_3$ solution, 5 g of KNO$_3$ and 40 cm^2 of working electrode surface) so to verify a possible modification of the final result after a simple scale-up.

Table 1
Synthesis of the Ag-TiO$_2$ samples.

Sample	Ag NPs loading (% by weight)	mol PVP / mol Ag$^+$	pH
1	0	–	–
2	8	3:1	12
3	8	50:1	12
4	8	3:1	4
5	8	1:1	4
6	8	1:1	12
7	8	1:1	12

2.3. Characterization

A JEOL 3010–UHR Instrument fitted with a LaB6 filament (acceleration potential 300 kV) and equipped with an Oxford INCA Energy TEM 200 energy dispersive X–ray (EDX) detector (TEM-HRTEM) imaged the samples. Samples were dry dispersed onto Cu grids coated with "lacey" carbon film.

A PANalytical Xpert Multipurpose X-ray Diffractometer measured samples crystallinity. It is equipped with a Cu anode (Kα radiation, λ = 1.54060 nm). The working potential was 45 kV while the working current was 40 mA. We analyzed our samples with a scan rate of 0.05° in a 2θ range of 20°-80°.

An M-Probe (SSI) XPS instrument was used to analyze the samples surfaces detecting in particular Ti$_{2p}$, O$_{1s}$ and Au$_{4f}$ regions. The instrument is equipped with a monochromatic Al$_{kα}$ anode and is calibrated using C$_{1s}$ at 284.6 eV.

Specific surface area measurements were carried out by conventional N$_2$ adsorption/desorption (BET) at 77 K by means of a Sorptometer (Costech Mod. 1042) apparatus.

A Thermo Scientific Evolution 600 spectrophotometer equipped with a diffuse reflectance accessory Praying-Mantis sampling kit measured the absorbance, (Harrick Scientific Products, USA). The reference material was a Spectralon1 disk.

2.4. NOx setup

We adopted a 20 L Pyrex glass batch reactor to degrade NOx. The complete description of the setup is reported elsewhere [33] and its scheme is available in the Supporting Information file (S4). We deposited a suspension of (0.050 ± 0.001) mg of catalyst in isopropanol (technical grade, Sigma Aldrich) on a glass plate (200 mm x 20 mm). An ultrasonic bath suspended the powder in the alcohol before the deposition. After the evaporation of the solvent, we placed the plate with the catalyst on the top of it inside the reactor. The concentration of the model pollutant was 500 ppb of NOx (initial bottle concentration 0.625% of NO$_2$ and 0.125% of NO, diluted with air). A LED lamp (MW mean well, 350 mA rated current, 9 V to 48 V DC voltage range, 16:8 W rated power) with emission from 400 nm to 700 nm was the photon source set at a distance to have 1000 lx on the sample surface. We set the relative humidity of the reactor at 50%. Time 0 corresponded to the switching on of the lamp. An Ecotech Serinus 40NOx directly connected to the reactor measured the concentration of both NO and NO$_2$ at 60, 180 and 360 min.

The calibration of the instrument was verified by sampling directly from the NOx cylinder to the instrument. The concentration of NOx matched the one declared by the gas supplier. The sampling was realized by opening a valve to let the instrument automatically withdraw a gas aliquot from the reactor. The lower detection limit of the instrument is 0.4 ppb and a precision of 0.5% [34]. Therefore, we calculated the error on the NOx conversion using the formula for the error propagation.

3. Results and discussion

3.1. Selection of the capping agent

The electrochemical synthesis of AgNPs failed with PAA and PVA for different reasons. The carboxylic domains of PAA exchanged sodium ion with silver ion in the solution and formed an insoluble complex that precipitated [35]. PVA did bring to the formation of an AgNPs solution, but that was in turn unstable. For all the concentrations tested, the NPs coagulated and aggregated within 3–4 h. Literature reports stability for the Ag-PVA complex with increasing dispersant molecular weight and when other rheological additives are present [36]. We filed the synthesis with different concentration of PVA (from 10 to 30 g L^{-1}). We therefore selected PVP for all the synthesis.

3.2. Sample morphology and nanoparticle size distribution

All the samples object of the present research exhibit almost the same value (~ 12 ± 2 m^2 g^{-1}) of BET specific surface area, i.e. the value related to the bare TiO$_2$ (micrometric sample 1) despite the presence of Ag NPS.

TEM confirmed that the average dimensions for sample 1 (i.e., bare Kronos 1077) are around 110 nm. Its particles are well ordered, in most cases they are thin and not too much closed packed together. Detailed inspection at higher magnification (see Supporting Information Fig S1) indicates that all the particles are highly crystalline: the calculated distances (0.35 nm) among the fringes evidence that the most frequently exposed crystal planes belong to the (101) family of anatase [ICDD 21-1272]. This feature is also confirmed by the analysis of the electron diffraction.

The general morphology of the supporting material remains unchanged for Sample 2, despite the procedure followed to add silver species. Sample 2 exhibits the same external habit of the titania crystals reported for sample 1 and the same fringe patterns ascribable to anatase (see Fig. 1b).

The extra particles present in Fig. 1a, characterized by a much lower size and higher contrast as well, are made up of Ag. This is confirmed by different experimental pieces of evidence: (i) the EDX analysis, reported in the inset to Fig. 1a, indicates the presence of metallic Ag, besides Ti and O; (ii) the inspection of the fringe patterns exhibited by the smaller particles (Fig. 1b) puts into evidence that the calculated 0.23 nm distances are ascribable to metallic silver [ICDD 004-0783]. Sample 3 resembles sample 2 (Fig. 2). Both samples have been synthesized in similar pH (basic) conditions but with different PVP.

Samples 4 and 5 were synthesized in acidic conditions. Their morphology confirms to be unaltered for the titania support, but deeply different for what concerns the Ag NPs appearance (see Figs. 3 and 4, respectively). In fact, their size is much smaller, being far beyond half than in the case of the samples obtained at basic pH.

In the case of sample 6, the situation is intermediate between the two above described: see Fig. 5. Sample 7 shows the same morphology of sample 6 confirming that the scale-up process does not alter the AgNPs features.

For samples 2, 3 and 6 (and 7) there is a broader spread of Ag NPs dimensions, ranging in the 5–25 nm (with dominating dimensions in the 15–20 nm range, Supporting Information Figure S2) with respect to samples 4 and 5, for which the distribution is much narrower and whose mean size is located in the 1–5 nm range.

The amount of silver in the various preparations (Table 1) was constant (8%$_{wt}$), whereas the parameters that have been changed are either the amount of the PVP dispersing agent or the pH of the solutions before the electrochemical synthesis.

In the condition of constant pH (no matter acidic or basic), the effect of a different amount of PVP is almost negligible, as the relevant AgNPs distribution is similar for the two pH values. Our results hold also considering diverse AgNPs preparation methods. Malina et al. [37]
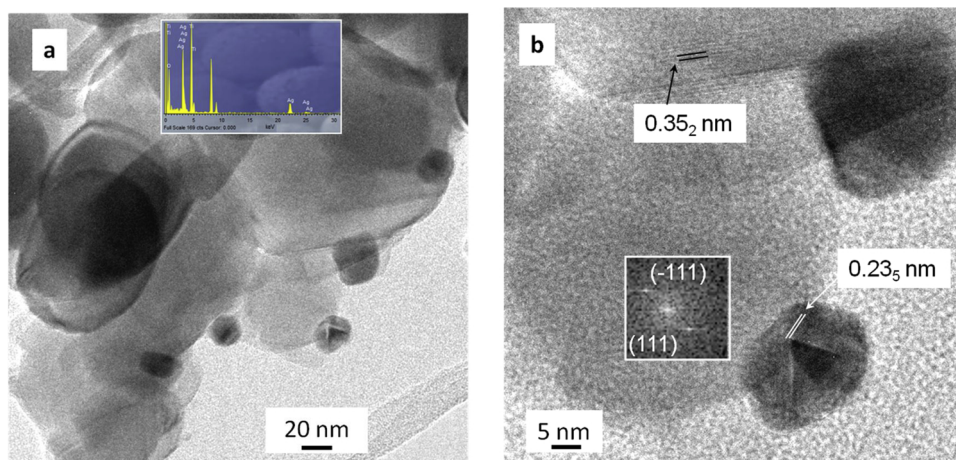
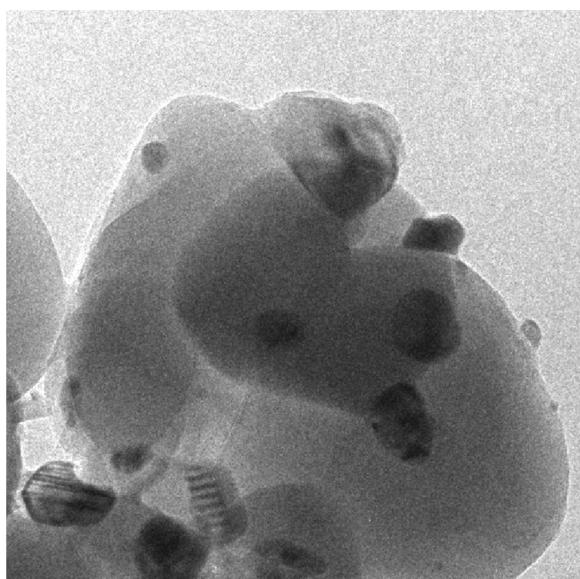**Fig. 1.** C-TEM (section a) and HR-TEM (section b) images referred to sample 2.

Fig. 2. C-TEM image referred to sample 3.

distribution during the laser ablation preparation method [38].

On the other hand, the different pH values have a great influence in the Ag NPs distributions. In fact, changing pH from 11.5–12.5 leads to bigger nanoparticles when the reducing agent is a sugar [39]. Therefore, pH possesses a leading role in determining the ultimate size(s) of the AgNPs, during the direct electrochemical reduction of AgNO$_3$.

The crystallographic phase composition of the various samples has been assessed also based on the X-Ray diffraction investigation: Fig. 6 summarizes the relevant results for the 2–5 powders.

It is well evident that the main features are ascribable to the anatase TiO$_2$ polymorph, as expected also on the basis of the morphological characterization carried out by means of HR-TEM investigation. In all the diffractograms, the main peak at 2θ– 25° can be ascribed to the most intense (101) peak due to anatase [ICDD card n. 21-1272], as well as many other reflexes: a few differences in intensity for the minor peaks is observable, but this is the only peculiarity that can be evidenced in particular for sample 4 and 5, synthesized in acidic conditions. Besides these peaks, a clear indication of the presence of metallic Ag comes from the three reflexes located at 2θ ˜ 38°, 44° and 65°, respectively ascribable to (111), (200) and (200) crystal planes [on the basis of metallic Ag ICDD card n. 4-0783]. No extra peaks are observable that can indicate the presence of oxidated Ag species: this fact may be due to the very low amount of these species (if present most likely due to passivation effects), lying then under the detection power of the XRD technique. For this reason, we resorted the XPS analysis in order to shed some light onto this feature.
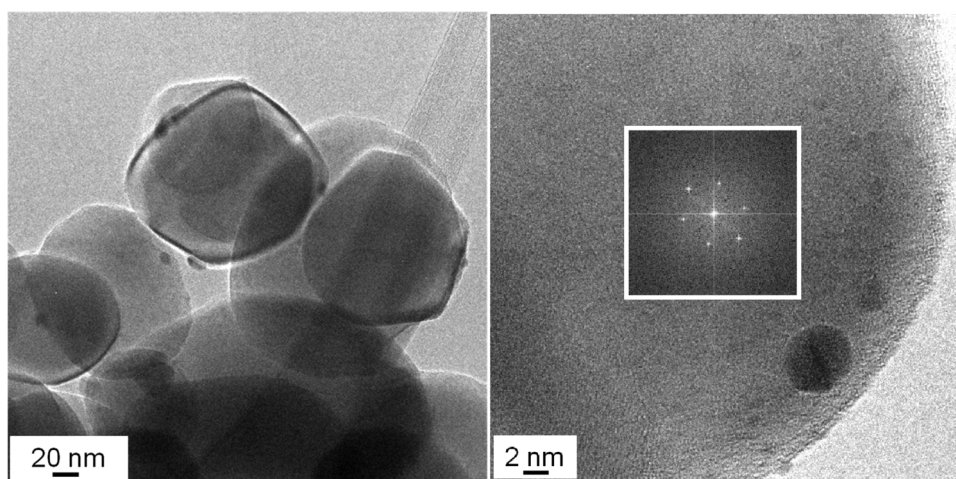
reduced AgNO$_3$ with NaBH$_4$ varying the concentration of PVP. They did not see a significant change in AgNPs size below a concentration of 10% of PVP. Moreover, changing PVP concentration leads to similar NPs

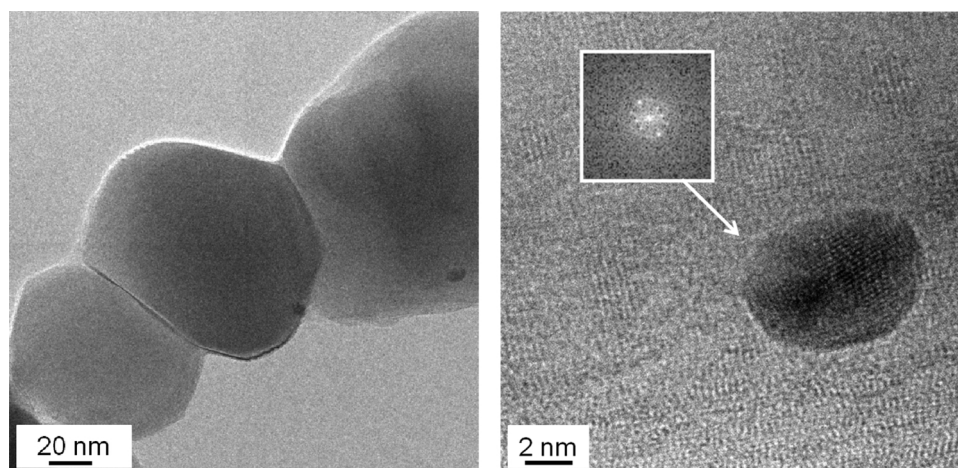**Fig. 3.** C-TEM (section a) and HR-TEM (section b) images referred to sample 4.

Fig. 4. C-TEM (section a) and HR-TEM (section b) images referred to sample 5.

High-resolution XPS for O 1 s region (sample 6) is the sum of three contributions: the main peak centred at 530 eV, representing the lattice oxygen of TiO$_2$, a less intense shoulder peak with binding energy at 531 eV, corresponding to the lattice oxygen of Ag$_x$O, and a third shoulder peak at 532 eV, related to OH species [40] (Fig. 7 right).

Ti 2p spectrum (Supporting Information, Figure S3) only highlights the presence of a single doublet typical of Ti^{4+} in TiO$_2$.

The ratio between the areas of the peaks located at 529 and 532 eV, respectively, gives useful information about the hydroxyl species (OH) located at the surface of the photocatalyst. In particular, if we compare the OH/O$_{tot}$ ratio calculated for samples 6 and 1 (bare TiO$_2$), we obtain 0.06 and 0.32 [36], respectively: on the basis of this evidence, we can preliminary conclude sample 6 activity is related to the creation of oxyradicals in situ, favoured because of controlled humidity (50%) (see the NOx degradation section).

The Ag3d XPS spectrum of sample 6 (Fig. 7 left) fits into two separated peaks, one referring to Ag° and the other one to its higher valence state Ag$^+$/Ag$_x$O [35]. The presence of higher valence state Ag confirms the deduction made discussing the O1s XPS spectrum, due to the presence of a fitted peak at ~531 eV. Due to the calcination in the air during the final preparation step, a mix of metal and oxidized Ag nanoparticles are present on the surface of the TiO$_2$ micro-particles. This morphological feature has not been evidenced by the HR-TEM inspection, as the fraction of oxidized AgNPs is most likely so low that lies under the detection power of this experimental technique.
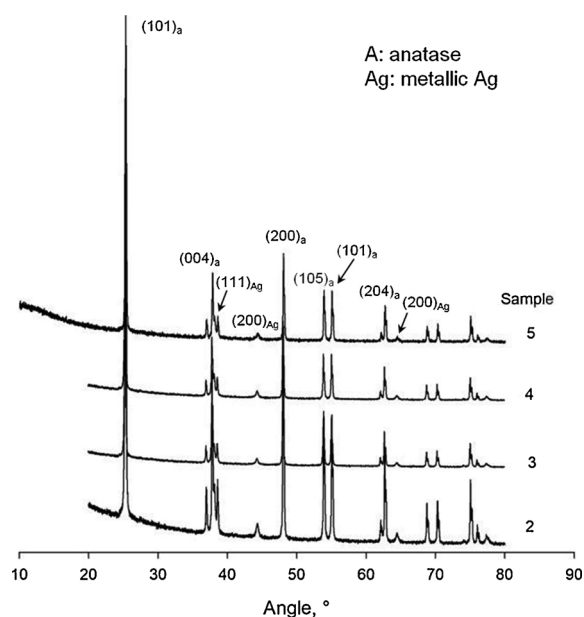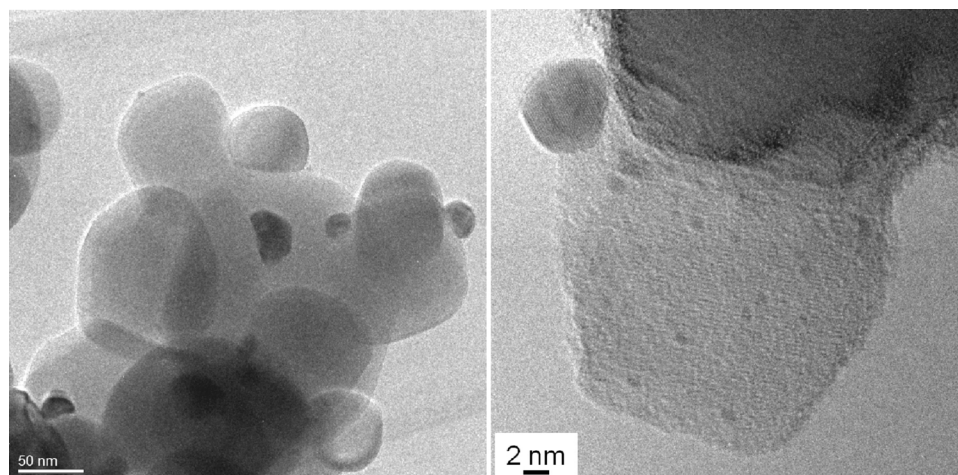

Fig. 6. XRD of samples 2–5.

Fig. 5. C-TEM (section a) and HR-TEM (section b) images referred to sample 6.
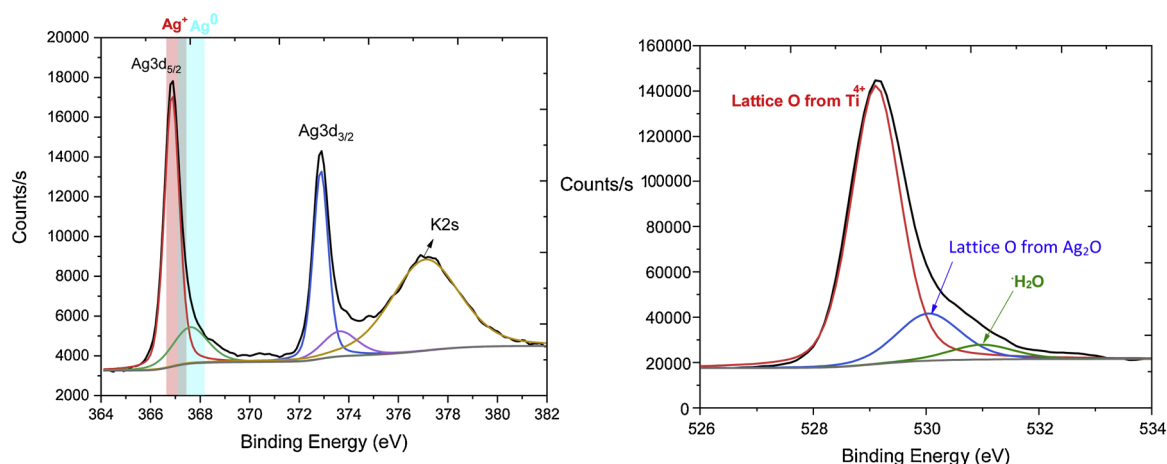
Fig. 7. XPS High-resolution spectrum of O1 s (right) and Ag3d (left) for sample 6.

A modification of the UV–vis spectra is also evident (supporting information, Figure S5) with an increase of the adsorption at wavelengths in the visible range of 400 nm and 700 nm for all samples but mainly for sample 6.

3.3. NOx degradation

Bare 1077 micro TiO_2 (sample 1) is ineffective towards NOx degradation under visible light. Our result is comparable to the literature and confirms that this material is only active under UV light [33].

Sample 2 exhibits exceptional activity. It converts 90% of NOx after 1 h of irradiation. Sample 3, 5 and 6 have similar kinetics, while sample 4 is the least active among the series (Fig. 8a). Sample 7 shows the same result of sample 6 even if it was prepared with 5 times the volumes of reagents. Therefore, the properties of this catalyst are unaffected by the volume of the synthesis.

All the catalysts tend to deactivate after 6 h due to the reaction mechanism that brings to the formation of nitrate species (NO_3^-), which we already detected in previous works employing photocatalytic tiles [33,41].

Ag NPs, as well as gold NPs, degrade VOC through different mechanisms depending on the light source and their morphology [42]. Here, we adopted LED light, whose energy is insufficient to directly promote electrons to the valance band of TiO_2. Therefore, localized surface plasmon resonance (LSPR) absorption in Ag NPs is the main effect that makes our samples active. However, when nanoparticles cluster, the absorption is broader and covers a wavelength range of 350–500, a range that falls in the emission of the LED lamp employed in
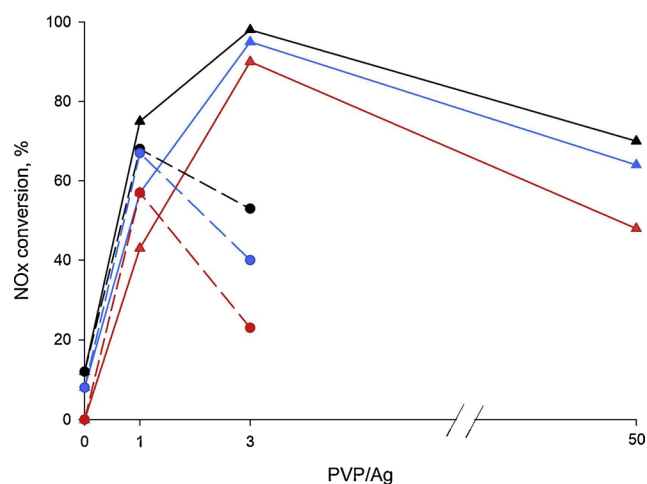

Fig. 9. PVP/Ag molar ratio versus NOx conversion for acid pH (dotted lines and points) and basic pH (full line and triangles). Red, blue and black lines represent conversion at time 1 h, 3 h, and 6 h, respectively. (For interpretation of the references to colour in this figure legend, the reader is referred to the web version of this article).

our study, which also contributes to their activity, even if to a lower extent.

The optimal PVP/Ag + molar ratio at pH = 4 was 1, while at pH = 12 it becomes 3 (Fig. 9). We hypothesize that this is connected to
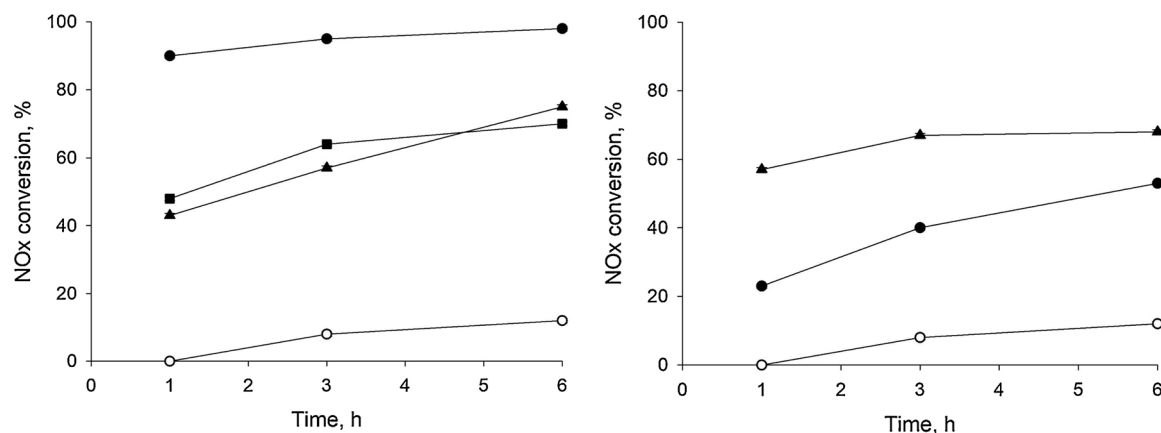

Fig. 8. NOx conversion versus time for catalysts prepared at basic (left side) and acid (right side) pH. Empty symbols correspond to Kronos 1077 while triangles, points and squares represent a PVP/Ag molar ratio of 1, 3 and 50, respectively.

the particle dimensions. At acid pH, smaller particles form (1–5 nm), therefore less PVP is needed to stabilize them, even though their number is higher, and as a matter of fact, an AgNP size smaller than 5 nm leads to lower NOx conversions.

Sarina et al. correlated the conversion of a photocatalytic reaction (ethylene oxidation) to the plasmon intensity [42]. In another work, Amendola et al. calculated the LSPR of different AgNPs, varying their shapes and assemblies [43]. A single spherical AgNP (radius = 10 nm) absorbs light whose wavelength is between 350 and 450 nm. The same authors also demonstrated that AgNPs smaller than 5 nm, like the ones we obtained in the synthesis with pH = 4, broaden the absorption band, which correlates with their lower performances compared to a catalyst prepared at basic pH.

4. Conclusion

In the present contribution, we synthesized AgNPs reducing silver nitrate in solution by an electrochemical method. The pH of the solution tailors the dimension of the nanoparticles. At pH = 4 we obtained a NPs distribution 1–5 nm, whereas at pH = 12 this figure becomes 5–25 nm. pH and polyvinyl pyrrolidone have no influence on the crystallinity of samples and the calcination procedure we propose (400 °C for 2 h in the air) yield stable nanoparticles.

As for the titania photocatalyst support, we decided to employ a micrometric commercial system (1077 by Kronos) rather than a nanometric powder, in order to avoid all the possible drawbacks typical of the interaction of NPs with human tissues by either inhalation or skin contact. The photocatalysts we obtained retain all the positive properties due to the micrometric support, such as SSA, crystallographic phase composition, being thus positively influenced in their photocatalytic performances by the promotion by AgNPs, even though a different photodegradation behaviour, as a function of the different AgNPs preparation route, has been put into evidence.

In particular, photocatalytic degradation of NOx under LED light evidence that the samples prepared at basic conditions exhibit better performances rather than those prepared at acid conditions: AgNPs with diameters of 1–5 nm are less active under LED light because of the broadening of the surface plasmon band. Moreover, the synthesis was scaled up to 500 mL volume, without affecting the final catalysts performances.

Appendix A. Supplementary data

Supplementary material related to this article can be found, in the online version, at doi:https://doi.org/10.1016/j.apcatb.2019.04.056.

References

[1] G. Mamba, J. Kiwi, C. Pulgarin, R. Sanjines, S. Giannakis, S. Rtimi, Evidence for the degradation of an emerging pollutant by a mechanism involving iso-energetic charge transfer under visible light, Appl. Catal. B Environ. 233 (2018) 175–183, https://doi.org/10.1016/j.apcatb.2018.03.109.

[2] C. Pirola, D.C. Boffito, S. Vitali, C.L. Bianchi, Photocatalytic coatings for building industry: study of 1 year of activity in the NO x degradation, J. Coatings Technol. Res. 9 (2012) 453–458, https://doi.org/10.1007/s11998-011-9381-7.

[3] M. Hosseini-Sarvari, F. Jafari, A. Mohajeri, N. Hassani, Cu 2 O/TiO 2 nanoparticles as visible light photocatalysts concerning C(sp 2)–P bond formation, Catal. Sci. Technol. 8 (2018) 4044–4051, https://doi.org/10.1039/C8CY00822A.

[4] Z. Wei, M. Janczarek, M. Endo, K. Wang, A. Balčytis, A. Nitta, M.G. Méndez-Medrano, C. Colbeau-Justin, S. Juodkazis, B. Ohtani, E. Kowalska, Noble metal-modified faceted anatase titania photocatalysts: octahedron versus decahedron, Appl. Catal. B Environ. 237 (2018) 574–587, https://doi.org/10.1016/j.apcatb. 2018.06.027.

[5] Z. Song, B. Hong, X. Zhu, F. Zhang, S. Li, J. Ding, X. Jiang, J. Bao, C. Gao, S. Sun, CdS/Au/Ti/Pb(Mg1/3Nb2/3)0.7Ti0.3O3 photocatalysts and biphotoelectrodes with ferroelectric polarization in single domain for efficient water splitting, Appl. Catal. B Environ. 238 (2018) 248–254, https://doi.org/10.1016/j.apcatb.2018.07. 033.

[6] N. Saadatkhah, M.G. Rigamonti, D.C. Boffito, H. Li, G.S. Patience, Spray dried SiO 2 WO 3 /TiO 2 and SiO 2 vanadium pyrophosphate core-shell catalysts, Powder Technol. 316 (2017) 434–440, https://doi.org/10.1016/j.powtec.2016.10.056.

[7] H. Khan, M.G. Rigamonti, G.S. Patience, D.C. Boffito, Spray dried TiO 2 /WO 3 heterostructure for photocatalytic applications with residual activity in the dark, Appl. Catal. B Environ. 226 (2018) 311–323, https://doi.org/10.1016/j.apcatb. 2017.12.049.

[8] Z. Wang, X. Lang, Visible light photocatalysis of dye-sensitized TiO2: the selective aerobic oxidation of amines to imines, Appl. Catal. B Environ. 224 (2018) 404–409, https://doi.org/10.1016/j.apcatb.2017.10.002.

[9] X. Li, J.-L. Shi, H. Hao, X. Lang, Visible light-induced selective oxidation of alcohols with air by dye-sensitized TiO 2 photocatalysis, Appl. Catal. B Environ. 232 (2018) 260–267, https://doi.org/10.1016/j.apcatb.2018.03.043.

[10] A. Utsunomiya, A. Okemoto, Y. Nishino, K. Kitagawa, H. Kobayashi, K. Taniya, Y. Ichihashi, S. Nishiyama, Mechanistic study of reaction mechanism on ammonia photodecomposition over Ni/TiO 2 photocatalysts, Appl. Catal. B Environ. 206 (2017) 378–383, https://doi.org/10.1016/j.apcatb.2017.01.045.

[11] I. Milošević, S. Rtimi, A. Jayaprakash, B. van Driel, B. Greenwood, A. Aimable, M. Senna, P. Bowen, Synthesis and characterization of fluorinated anatase nanoparticles and subsequent N-doping for efficient visible light activated photocatalysis, Colloids Surf. B Biointerfaces 171 (2018) 445–450, https://doi.org/10. 1016/j.colsurfb.2018.07.035.

[12] S. Rtimi, D.D. Dionysiou, S.C. Pillai, J. Kiwi, Advances in catalytic/photocatalytic bacterial inactivation by nano Ag and Cu coated surfaces and medical devices, Appl. Catal. B Environ. 240 (2019) 291–318, https://doi.org/10.1016/j.apcatb.2018.07. 025.

[13] A. Moores, F. Goettmann, The plasmon band in noble metal nanoparticles: an introduction to theory and applications, New J. Chem. 30 (2006) 1121, https://doi. org/10.1039/b604038c.

[14] Q. Lang, Y. Chen, T. Huang, L. Yang, S. Zhong, L. Wu, J. Chen, S. Bai, Graphene "bridge" in transferring hot electrons from plasmonic Ag nanocubes to TiO2 nanosheets for enhanced visible light photocatalytic hydrogen evolution, Appl. Catal. B Environ. 220 (2018) 182–190, https://doi.org/10.1016/j.apcatb.2017.08.045.

[15] R. Asapu, N. Claes, S. Bals, S. Denys, C. Detavernier, S. Lenaerts, S.W. Verbruggen, Silver-polymer core-shell nanoparticles for ultrastable plasmon-enhanced photocatalysis, Appl. Catal. B Environ. 200 (2017) 31–38, https://doi.org/10.1016/j. apcatb.2016.06.062.

[16] A. Jbeli, Z. Hamden, S. Bouattour, A.M. Ferraria, D.S. Conceição, L.F.V. Ferreira, M.M. Chehimi, A.M.B. do Rego, M. Rei Vilar, S. Boufi, Chitosan-Ag-TiO2 films: an effective photocatalyst under visible light, Carbohydr. Polym. 199 (2018) 31–40, https://doi.org/10.1016/j.carbpol.2018.06.122.

[17] M. Stucchi, C.L. Bianchi, C. Argirusis, V. Pifferi, B. Neppolian, G. Cerrato, D.C. Boffito, Ultrasound assisted synthesis of Ag-decorated TiO2 active in visible light, Ultrason. Sonochem. 40 (2018) 282–288, https://doi.org/10.1016/j.ultsonch. 2017.07.016.

[18] Q. Zeng, X. Xie, X. Wang, Y. Wang, G. Lu, D.Y.H. Pui, J. Sun, Enhanced photocatalytic performance of Ag@TiO2 for the gaseous acetaldehyde photodegradation under fluorescent lamp, Chem. Eng. J. 341 (2018) 83–92, https://doi.org/10.1016/ j.cej.2018.02.015.

[19] M. Starowicz, B. Stypuła, J Banaś, Electrochemical synthesis of silver nanoparticles, Electrochem. commun. 8 (2006) 227–230, https://doi.org/10.1016/j.elecom.2005. 11.018.

[20] K. Ozawa, M. Emori, S. Yamamoto, R. Yukawa, S. Yamamoto, R. Hobara, K. Fujikawa, H. Sakama, I. Matsuda, Electron–hole recombination time at TiO 2 single-crystal surfaces: influence of surface band bending, J. Phys. Chem. Lett. 5 (2014) 1953–1957, https://doi.org/10.1021/jz500770c.

[21] F. Hong, L. Wang, Nanosized titanium dioxide-induced premature ovarian failure is associated with abnormalities in serum parameters in female mice, Int. J. Nanomedicine 13 (2018) 2543–2549, https://doi.org/10.2147/IJN.S151215.

[22] P. Sá-Pereira, M.S. Diniz, L. Moita, T. Pinheiro, E. Mendonça, S.M. Paixão, A. Picado, Protein profiling as early detection biomarkers for TiO2 nanoparticle toxicity in Daphnia magna, Ecotoxicology 27 (2018) 430–439, https://doi.org/10. 1007/s10646-018-1907-7.

[23] M. Stucchi, D. Boffito, E. Pargoletti, G. Cerrato, C. Bianchi, G. Cappelletti, Nano-MnO2 decoration of TiO2 microparticles to promote gaseous ethanol visible photoremoval, Nanomaterials 8 (2018) 686, https://doi.org/10.3390/nano8090686.

[24] G. Cerrato, C.L. Bianchi, F. Galli, C. Pirola, S. Morandi, V. Capucci, Micro-TiO2 coated glass surfaces safely abate drugs in surface water, J. Hazard. Mater. 363 (2019) 328–334, https://doi.org/10.1016/j.jhazmat.2018.09.057.

[25] M. Stucchi, C.L. Bianchi, C. Pirola, S. Vitali, G. Cerrato, S. Morandi, C. Argirusis, G. Sourkouni, P.M. Sakkas, V. Capucci, Surface decoration of commercial micro-sized TiO2 by means of high energy ultrasound: a way to enhance its photocatalytic activity under visible light, Appl. Catal. B Environ. 178 (2015) 124–132, https:// doi.org/10.1016/j.apcatb.2014.10.004.

[26] Ambient (outdoor) Air Quality and Health, WHO, 2018 (Accessed February 1, 2019), https://www.who.int/news-room/fact-sheets/detail/ambient-(outdoor)-air-quality-and-health.

[27] A. Folli, J.Z. Bloh, M. Strøm, T. Pilegaard Madsen, T. Henriksen, D.E. Macphee, Efficiency of Solar-Light-Driven TiO 2 Photocatalysis at Different Latitudes and Seasons. Where and When Does TiO 2 Really Work? J. Phys. Chem. Lett. 5 (2014)

830–832, https://doi.org/10.1021/jz402704n.

[28] M. Schreck, M. Niederberger, Photocatalytic gas phase reactions, Chem. Mater. (2019), https://doi.org/10.1021/acs.chemmater.8b04444 acs.chemmater. 8b04444.

[29] N. Bowering, G.S. Walker, P.G. Harrison, Photocatalytic decomposition and reduction reactions of nitric oxide over Degussa P25, Appl. Catal. B Environ. 62 (2006) 208–216, https://doi.org/10.1016/j.apcatb.2005.07.014.

[30] B. Yin, H. Ma, S. Wang, S. Chen, Electrochemical synthesis of silver nanoparticles under protection of poly(N -vinylpyrrolidone), J. Phys. Chem. B 107 (2003) 8898–8904, https://doi.org/10.1021/jp0349031.

[31] R. Surudzic, Z. Jovanovic, N. Bibic, B. Nikolic, V. Miskovic-Stankovic, Electrochemical synthesis of silver nanoparticles in poly(vinyl alcohol) solution, J. Serbian Chem. Soc. 78 (2013) 2087–2098, https://doi.org/10.2298/JSC131017124S.

[32] S. Magdassi, M. Grouchko, O. Berezin, A. Kamyshny, Triggering the sintering of silver nanoparticles at room temperature, ACS Nano 4 (2010) 1943–1948, https://doi.org/10.1021/nn901868t.

[33] C.L. Bianchi, C. Pirola, F. Galli, G. Cerrato, S. Morandi, V. Capucci, Pigmentary TiO2: a challenge for its use as photocatalyst in NOx air purification, Chem. Eng. J. 261 (2015) 76–82, https://doi.org/10.1016/j.cej.2014.03.078.

[34] Serinus 40 Brochure, Ecotech, 2018, p. 2 (Accessed January 21, 2019), https://www.ecotech.com/wp-content/uploads/2015/03/ECOTECH-Serinus-40-NOx-Gas-Analyser-spec-sheet-20181202.pdf.

[35] J.A. Dean, Lange's Handbook Of Chemistry, 15th ed., (1999).

[36] K.A. Juby, C. Dwivedi, M. Kumar, S. Kota, H.S. Misra, P.N. Bajaj, Silver nano-particle-loaded PVA/gum acacia hydrogel: synthesis, characterization and antibacterial study, Carbohydr. Polym. 89 (2012) 906–913, https://doi.org/10.1016/j.carbpol.2012.04.033.

[37] D. Malina, A. Sobczak-Kupiec, Z. Wzorek, Z. Kowalski, Silver nanoparticles synthesis with different concentrations of Polyvinylpyrrolidone, Dig. J. Nanomater. Biostruct. 7 (2012) 1527–1534.

[38] T. Tsuji, D.-H. Thang, Y. Okazaki, M. Nakanishi, Y. Tsuboi, M. Tsuji, Preparation of silver nanoparticles by laser ablation in polyvinylpyrrolidone solutions, Appl. Surf. Sci. 254 (2008) 5224–5230, https://doi.org/10.1016/j.apsusc.2008.02.048.

[39] A. Panáček, L. Kvítek, R. Prucek, M. Kolář, R. Večeřová, N. Pizúrová, V.K. Sharma, T. Nevěčná, R. Zbořil, Silver colloid nanoparticles: synthesis, characterization, and their antibacterial activity, J. Phys. Chem. B 110 (2006) 16248–16253, https://doi.org/10.1021/jp063826h.

[40] H. Ren, P. Koshy, F. Cao, C.C. Sorrell, Multivalence charge transfer in doped and codoped photocatalytic TiO 2, Inorg. Chem. 55 (2016) 8071–8081, https://doi.org/10.1021/acs.inorgchem.6b01200.

[41] C.L. Bianchi, C. Pirola, F. Galli, S. Vitali, A. Minguzzi, M. Stucchi, F. Manenti, V. Capucci, NO x degradation in a continuous large-scale reactor using full-size industrial photocatalytic tiles, Catal. Sci. Technol. 6 (2016) 2261–2267, https://doi.org/10.1039/C5CY01627D.

[42] S. Sarina, E.R. Waclawik, H. Zhu, Photocatalysis on supported gold and silver nanoparticles under ultraviolet and visible light irradiation, Green Chem. 15 (2013) 1814, https://doi.org/10.1039/c3gc40450a.

[43] V. Amendola, O.M. Bakr, F. Stellacci, A study of the surface Plasmon resonance of silver nanoparticles by the discrete dipole approximation method: effect of shape, size, structure, and assembly, Plasmonics 5 (2010) 85–97, https://doi.org/10.1007/s11468-009-9120-4.